Journal of proteome research

Open Access

pubs.acs.org/jpr

Article

Analysis of Stratifin Expression and Proteome Variation in a Rat Model of Acute Lung Injury

Ayaka Yoshida, Yuya Hashimoto, Hirotoshi Akane, Shinichiro Matsuyama, Takeshi Toyoda, Kumiko Ogawa, Yoshiro Saito, Ruri Kikura-Hanajiri, and Noriaki Arakawa*

Cite This: J. Proteome Res. 2025, 24, 1941−1955

Read Online

ACCESS | Metrics & More | Article Recommendations | Supporting Information

ABSTRACT: Diffuse alveolar damage (DAD) is a pathological hallmark of severe interstitial lung diseases, such as acute respiratory distress syndrome (ARDS), and is linked to poor prognosis. Previously, we identified 14−3−3σ/stratifin (SFN) as a serum biomarker candidate for diagnosing DAD. To clarify the time-dependent relationship between SFN expression and DAD, we here investigated pathological and molecular changes in serum, bronchoalveolar lavage fluid (BALF), and lung tissue in an oleic acid (OA)-induced ARDS rat model. Acute alveolar edema was observed after OA administration, followed by alveolar epithelial cell proliferation and increased BALF and serum SFN levels. Proteomic analysis of lung tissue extracts revealed that proteins related to "inflammatory response" and "HIF-1 signaling," including plasminogen activator inhibitor-1, were markedly increased 3 h after acute lung injury, followed by a gradual decrease. Conversely, proteins associated with "cell cycle" and "p53 pathway," including SFN, showed a persistent increase starting at 3 h and peaking at 48 h. Western blotting and immunohistochemistry confirmed that SFN was expressed in a part of proliferated alveolar type-II cells, accompanied by p53 activation, an important event for differentiation into type-I cells. SFN may be a biomarker closely related to alveolar remodeling during the repair process after lung injury.

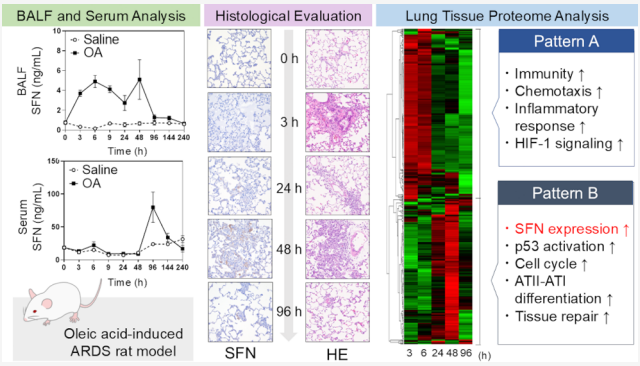

KEYWORDS: *diffuse alveolar damage, interstitial lung disease, acute lung injury, acute respiratory distress syndrome, stratifin, oleic acid, proteomics, biomarker*

INTRODUCTION

Interstitial lung disease (ILD) encompasses various types of conditions classified by histological patterns. The most severe type is diffuse alveolar damage (DAD). DAD is typically observed in patients with acute lung injury—such as in acute exacerbation of idiopathic pulmonary fibrosis (IPF), acute respiratory distress syndrome (ARDS), and severe coronavirus disease 2019 (COVID-19)—and it often occurs as an adverse reaction to anticancer drugs such as epidermal growth factor receptor-tyrosine kinase inhibitors (EGFR-TKIs).[1] Patients with DAD do not sufficiently respond to treatment, leading to a poor prognosis. Because DAD progression leads to irreversible fibrosis of the lungs, early diagnosis and treatment are crucial for improving patient outcomes.[2] Surfactant protein (SP)-D and Krebs von den Lungen-6 (KL-6) have been used as biomarkers in the diagnosis of drug-induced ILD (DILD). However, because elevations in these proteins are broadly observed in many types of ILD, blood biomarkers that can specifically diagnose DAD are urgently needed.

Previously, we applied aptamer-based proteomics to blood samples from patients with drug-induced ILD, and identified stratifin (14−3−3σ, SFN) as a novel serum diagnostic marker for DAD.[3] We then used our established in-house enzyme-linked immunosorbent assay (ELISA) to verify that serum SFN levels were indeed elevated in patients with DAD. Moreover, we showed that SFN was superior to KL-6 and SP-D in distinguishing DILD patients with DAD from those with non-DAD patterns.[3] Serum SFN is also known to be increased in patients with severe COVID-19 or acute exacerbation of IPF.[2,4] However, for practical use of SFN as a DAD biomarker in drug development and clinical settings, more evidence of a direct relationship between DAD pathology and SFN expression is needed. To demonstrate that SFN is not merely an inflammation biomarker but a definitive biomarker for DAD, it is essential to elucidate the biological and pathological processes associated with SFN, in addition to evaluating its diagnostic performance, including sensitivity and specificity, and its clinical validity.

Received: November 2, 2024
Revised: January 31, 2025
Accepted: February 12, 2025
Published: February 28, 2025

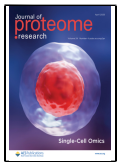

https://doi.org/10.1021/acs.jproteome.4c00980
J. Proteome Res. 2025, 24, 1941−1955

SFN belongs to the 14−3−3 family, which includes six other isoforms: β, γ, ε, ζ, η, and τ. This family is a group of highly evolutionarily conserved proteins with a molecular mass of 25−30 kDa and is found in all eukaryotes. These proteins modulate various cellular processes by binding to phosphorylated proteins.[5] While most 14−3−3 isoforms are expressed in various normal tissues in a ubiquitous manner, SFN is expressed in specific epithelia, such as skin and esophageal tissues.[5] SFN is a direct transcriptional target of p53, which is induced in response to DNA damage, and leads to the arrest of the G2/M phase of the cell cycle.[6] Moreover, an experiment using cultured human keratinocyte cells found that the upregulation of SFN is closely related to a reduction in cell proliferation and the progression of cellular senescence.[5] Despite increasing knowledge of the function of SFN, the relationship between ILD and SFN remains largely unclear. However, recent single-cell RNA-sequencing analysis has indicated that during the repair process of alveolar epithelium following acute lung injury, p53 activation plays an important role in the differentiation from alveolar epithelial type-II (ATII) cells to type-I (ATI) cells, and SFN is expressed during this process.[7−9]

The pathological features of DAD change consistently and dynamically in the early exudative, midproliferative (organizing), and late fibrotic phases following lung injury. Multiple cell types, such as immune cells, lung epithelial cells, endothelial cells, and fibroblasts, are involved in regulating the repair process after lung injury. After lung injury, ATII cells progress through a stepwise process comprising proliferation, transition into an ATII−ATI intermediate state (known as the prealveolar type-I transitional cell state (PATS)) and finally differentiation.[7−9] ATII cell proliferation is a regenerative response after injury. However, abnormal ATII cell proliferation can also be pathological and may lead to hyperplasia, which is also found in the proliferative phase during DAD progression. Therefore, in order to clarify the clinical significance of serum SFN as a DAD biomarker, it is necessary to first determine the mechanisms and temporal aspects of SFN expression and release from lung cells during DAD progression. However, clinical studies can only partially unravel these features; analysis of SFN in an animal model is essential to complement the clinical data. Furthermore, proteomics data comparing the behaviors of SFN and other proteins could lead to a more fundamental understanding of the relationship between SFN expression and DAD.

Among various animal models of lung injury,[10−12] the acute lung injury model induced by oleic acid (OA) exhibits acute and repair phases with histopathological features similar to those of human DAD/ARDS.[11,13] This study aimed to investigate whether the levels of SFN in the blood, BALF, and lung tissue are altered in the OA-induced ARDS rat model. By comparing the temporal changes in the pathological features and the proteome of lung tissue, we intended to clarify when, where, and with what proteins SFN is expressed in DAD-type ILD. Our final goal was to elucidate the specific expression of SFN in DAD lungs, its relationship with associated protein groups, and the physiological significance of this relationship, thereby contributing to a deeper understanding of the molecular mechanisms underlying DAD.

EXPERIMENTAL PROCEDURES

Animals

Eight−week−old male Crl:CD (Sprague−Dawley) rats were obtained from The Jackson Laboratory Japan (Kanagawa, Japan) and housed under controlled conditions: a temperature of 22 °C ± 3 °C, 55% ± 15% humidity, and a 12-h light/dark cycle. The rats had ad libitum access to food and water. They were randomly assigned to either a saline (1.25 mL/kg) or 0.1% bovine serum albumin-OA (0.25 mg/kg) treatment group. A single injection was administered via the tail vein at a rate of approximately 1 mL/min. Saline was purchased from Otsuka Pharmaceutical Factory (Tokyo), bovine serum albumin (BSA) was purchased from EMD Millipore (St. Louis, MO), and OA was purchased from Sigma-Aldrich (St. Louis, MO). At the end of the observation period, the rats were sacrificed by bloodletting under isoflurane (Mylan Inc., Tokyo) anesthesia using a NARCOBIT-E device (Natsume Seisakusho, Tokyo) and then necropsied. Blood samples were collected from the abdominal aorta using BD Vacutainer serum separator tubes (Nippon Becton Dickinson Company, Tokyo) and centrifuged at 3000g for 10 min at 15−24 °C. Serum aliquots were stored at −70 °C until use. BALF was collected from the right lung. After cannulating and ligating the trachea, 4.0 mL of sterile saline at room temperature was twice injected into the right lung lobe and spontaneously drained through the cannulated tube each time. After the BALF was collected, the right lungs were frozen with liquid nitrogen and stored at −70 °C until the protein and mRNA extracts were prepared. The left lungs were immunohistochemically stained after fixing with formalin. All animal experiments were conducted by the DIMS Institute of Medical Science (Aichi, Japan; this facility is currently closed).

This study was conducted in compliance with the "Act on Welfare and Management of Animals" (Act No. 39 of June 2009), the "Standards for the Care and Management of Laboratory Animals and Relief Pain" (Science Council of Japan, June 2006), and the guidelines established by the Ministry of Health, Labour, and Welfare and the Ministry of Agriculture, Forestry, and Fisheries. The study was approved by the Animal Care and Utilization Committee of the National Institute of Health Sciences (no. 832; September 15, 2021), and the DIMS Institute of Medical Science (no. 22507; January 28, 2022).

BALF Testing

The collected BALF was immediately centrifuged and separated into supernatant and sediment portions. The supernatant portion was analyzed using an automated analyzer (Hitachi High-Tech, Tokyo) for lactate dehydrogenase (LDH) concentration according to the Japan Society Clinical Chemistry (JSCC) method and for micrototal protein (μ-TP) concentration using the pyrogallol red method. The remaining supernatant was stored at −70 °C until use for ELISA-based biomarker assays. The sediment was mixed with 1 mL of sterile saline, and subjected to flow cytometry with a Xt-2000i multiparameter automated hematology analyzer.

ELISA

SFN levels in the BALF supernatant and serum were measured using an in-house ELISA method with two anti-SFN mAbs (clone CS112-2A8 [#05-632, Merck, Kenilworth, NJ] and clone 3c3 [#WH0000286M1, Sigma-Aldrich]), as previously described.[3] SP-D and albumin (ALB) levels were measured using the rat/mouse SP-D kit YAMASA EIA (Yamasa, Chiba, Japan) and rat ALB ELISA kit (Abnova, Taipei, Taiwan), respectively.

https://doi.org/10.1021/acs.jproteome.4c00980
J. Proteome Res. 2025, 24, 1941−1955

Protein Extraction

Protein was extracted from frozen lung tissues in RIPA buffer (FUJIFILM Wako Pure Chemical, Osaka, Japan) containing a protease inhibitor cocktail (Nacalai Tesque, Kyoto, Japan) using a polytron homogenizer (Central Scientific Commerce, Tokyo). After centrifugation at 3000 × *g* for 10 min at 4 °C, the supernatants were used for proteome and Western blot analyses.

Proteome Analysis

To precipitate protein for desalting and concentration, four times the volume of acetone was added to the protein extract. The resulting precipitate was then redissolved. Trypsin digestion and peptide cleanup were performed with a mass spectrometry (MS) sample preparation kit (EasyPep Mini MS Sample Prep Kits; Thermo Fisher Scientific, Waltham, MA), according to the manufacturer's instructions. The resulting peptides were analyzed using a data-independent acquisition (DIA) mode on a Q Exactive HF coupled with a Vanquish Neo LC System (Thermo Fisher Scientific). The peptides were loaded onto a 75 μm × 12 cm nano-LC column (Nikkyo Technos, Tokyo) and separated using a 115 min gradient. Solvent A contained 0.1% formic acid in water, and solvent B contained 0.1% formic acid in 100% acetonitrile. The gradient consisted of the following steps: for the first min, 5% solvent B; at 116 min, 36% solvent B; at 126 min, 90% solvent B; and at 135 min, 90% solvent B at a flow rate of 300 nL/min. In the DIA mode analysis, MS1 spectra were collected over a range of 495−745 m/z with a resolution of 60,000. The automatic gain control target was set to 3×10^6, using positive polarity and a maximum injection time of 100 ms. MS2 spectra were collected at 45,000 resolutions to set an automatic gain control target of 3×10^6, and the maximum injection time was set to "auto." The isolation width for MS2 was set to 4.0 m/z. For data analysis, the raw data files were converted to mzML files (with default parameters) using ProteoWizard (version: 3.0.23240). Peptides and proteins were identified and quantified from each converted mzML file using DIA-NN software (version 1.8.1, https://github.com/vdemichev/DiaNN). A spectral library for the search was generated from the *Rattus norvegicus* (Brown Norway rat) protein sequence database (UniProt id UP000002494; 22,401 (download one protein sequence per) gene entries) using DIA-NN. The search parameters were as follows: protease, trypsin/P; missed cleavages, 1; peptide length range, 7−30 amino acids; precursor charge range, 1−4; fragment ion m/z range, 200−1800; mass accuracy, auto (0.0); variable modification, loss of N-term methionine, cysteine carbamidomethylation; and "Heuristic protein inference" and "Use isotopologues" enabled. The peptide and protein FDR values were set to < 1%.

Bioinformatics Analysis

The missing values and statistical analysis of the MS signals were processed using Perseus (version 2.0.11.0; Max Planck Institute of Biochemistry, Planegg, Germany), and a volcano plot was generated. Differential proteins were selected using a threshold, which was set with a p-value < 0.05 (n = 3, Welch's t test) and a fold change of 1.0 compared with the pretreated group. The Database for Annotation, Visualization, and Integrated Discovery (DAVID) Knowledgebase v2024q2 (https://david.ncifcrf.gov/) was used for functional annotation of the differential proteins identified. The heatmap of the differential proteins was generated using the open-source package Heatmapper (http://www.heatmapper.ca/expression/). The settings were as follows: clustering method, Average linkage; Distance measurement method, Pearson. Each row represents one gene and each column represents the average of triplicate samples.

RNA Extraction and Real-Time qPCR Analysis

Total RNA was extracted from the frozen rat-lung tissues using an ISOGEN kit with Spin Column (Nippon Gene, Tokyo) and a polytron homogenizer (Central Scientific Commerce, Tokyo). The extracted total RNA was used for expression analysis of rat *Sfn*, *Serpine1*, cyclin-dependent kinase inhibitor 1A (*Cdkn1a*), and TATA box−binding protein (*Tbp*) genes using a One Step TB Green PrimeScript RT-PCR Kit II (Takara Bio, Shiga, Japan) and 7500 Fast Real-Time PCR System (Thermo Fischer Scientific, Waltham, MA). The expression level of each target gene was normalized to that of *Tbp*.

PCR primers with the following sequences were used:
Sfn-F; 5′-TGACGACAAGAAGCGCATCAT-3′
Sfn-R; 5′-GTAGTGGAAGACGGAAAAGTTCA-3′
Serpine1-F; 5′-ATCAACGACTGGGTGGAGAG-3′
Serpine1-R; 5′-CAGGCGTGTCAGCTCATTTA-3′
Cdkn1a-F; 5′-TAGGACTTCGGGGTCTCCTT-3′
Cdkn1a-R; 5′-GCTCTGGACGGTACGCTTAG-3′
Ctgf-F; 5′-GGGTCTCTTCTGCGACTTC-3′
Ctgf-R; 5′-ATCCAGGCAAGTGCACTGGTA-3′
Tbp-F; 5′-TGTAAACTTGACCTAAAGACCAT-3′
Tbp-R; 5′-CAGCAAACCGCTTGGGAT-3′

Western Blot Analysis

Protein extracts were separated using 5%−10% m-PAGEL (Atto, Tokyo) and transferred onto Trans-Blot Turbo Mini 0.2 μm PVDF Transfer Packs (Bio-Rad Laboratories, Hercules, CA). For detecting each protein, the following rabbit monoclonal antibodies (mAb) or polyclonal antibodies (pAb) were used: rabbit anti-plasminogen activator inhibitor-1 (PAI-1) pAb (#27535, Cell Signaling Technology, Leiden, The Netherlands; 1:1000) rabbit anti-p53 mAb (clone E9B5W [#30313, Cell Signaling Technology; 1:2000]), rabbit anti-phospho-p53 Ser15 pAb (#9284, Cell Signaling Technology; 1:2000), and β-actin rabbit pAb (#20536−1-A, Proteintech, Rosemont, IL; 1:5000). To detect these rabbit antibodies, the HRP-conjugated goat antirabbit IgG (#7074, Cell Signaling Technology; 1:5000) was used as the secondary antibody. For detecting SFN, mouse anti-SFN mAb clone 3c3 (#WH0002810M1, Sigma-Aldrich; 1:2000) was labeled with HRP using a peroxidase labeling kit (Dojindo, Kumamoto, Japan), and Streptavidin PolyHRP (Funakoshi, Tokyo; 1:20,000). Chemiluminescence was detected using the FUSION Solo S detection system (Vilber, Collégien, France) along with ECL select HRP substrate reagent (GE Healthcare, Uppsala, Sweden).

Immunohistochemical Staining

To investigate the expression and localization of SFN and Ki67, immunohistochemical analysis was performed using rat-lung tissue. The tissue sections were deparaffinized, hydrated, and autoclaved at 121 °C for 15 min for antigen retrieval in a 10 mM citrate buffer (pH 6.0). To inactivate endogenous peroxidase activity, the sections were immersed in a 3% H_2O_2/methanol solution for 10 min at room temperature. After blocking nonspecific reactions with 10% normal goat serum, the sections were incubated overnight at 4 °C with a primary antibody targeting SFN (diluted 1:2000; rabbit anti-SFN polyclonal antibody [HPA011105, Atlas Antibodies, Bromma, Sweden]) and Ki67 (diluted 1:1000; rabbit anti-Ki67 polyclonal antibody [ab15580, Abcam, Cambridge, UK]). Antibody binding was visualized using a VectaStain Elite ABC Kit (Vector

https://doi.org/10.1021/acs.jproteome.4c00980
J. Proteome Res. 2025, 24, 1941−1955

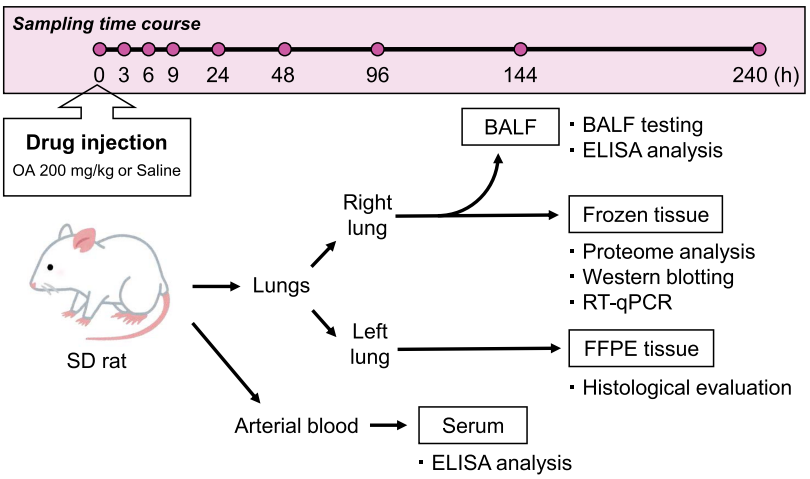

Figure 1. Schematic view of the animal experiment. Rats were intravenously injected with OA or saline, and their samples were collected at each time point (0, 3, 6, 9, 24, 48, 96, 144, and 240 h; $n = 5$ or 6). BALF was collected from the right lung. After BALF collection, the right lung tissues were frozen until the protein and RNA extraction. The left lung was paraffin-embedded for histological evaluation. Arterial blood was collected, and serum was separated. These samples were used for the indicated experiments.

Laboratories, Newark, CA) for SFN and a Histofine Simple Stain Rat MAX PO Kit (Nichirei Corporation, Tokyo) for Ki67. All sections were incubated with 3,3′-diaminobenzidine and counterstained with hematoxylin.

Statistical Analysis

All data were analyzed using GraphPad PRISM (version 8.4.3; GraphPad Software, San Diego, CA) and Perceus (Max Planck Institute of Biochemistry) software and are expressed as mean ± standard error of the mean (SEM) or standard deviation (SD). The statistical evaluation of the temporal change for each test value between the groups was performed using one-way (for the OA group only) or two-way (for the OA and control groups) ANOVA, followed by Dunnett's posthoc test and Bonferroni's posthoc test for multiple comparisons, respectively. Assumptions for ANOVA, including normality and homogeneity of variances, were tested using Shapiro-Wilk and Brown-Forsythe tests, respectively. The changes in protein levels based on DIA-MS data and the comparison of the SFN/ALB ratio in BALF and serum at each time point were evaluated using Welch's t test. Statistical significance was defined as a p-value < 0.05.

RESULTS

Characteristics of OA-Induced ARDS Rats

In the current study, the OA-induced ARDS rat model was used as an acute lung injury model to analyze the relationship between DAD and SFN in detail. After injecting OA intravenously, rat-lung tissues, BALF, and sera were collected at each time point (Figure 1).

The lung weight/body weight ratio, an indicator of lung inflammation in lung injury, showed a considerable increase 3 h after OA injection (Figure 2A). This was followed by a time-dependent decrease, and then recovery to the same level as in the pretreated group at 96 h. In the BALF collected from lung tissues of the OA group, LDH (an indicator of cell injury) and μ-TP (an indicator of vascular permeability) showed a pattern of change similar to the lung weight/body weight ratio (Figure 2B, C). Leukocytes and neutrophils also showed a rapid increase at 3 h (Figure 2D,E), while lymphocytes, eosinophils, and monocytes showed a gradual increase, peaking at 24 or 48 h after OA injection (Figure 2F−H). All immune cells recovered to nearly normal levels by 96 h.

Hematoxylin and eosin staining of lung tissues revealed that edema and hemorrhage occurred within 3 h after OA administration, along with the infiltration and accumulation of inflammatory cells around blood vessels by 24 h (Figure 2I). At 48 h, edema and hemorrhage were scarcely found, but many proliferated alveolar type-II (ATII) cells were observed. After 96 h, most of the tissue inflammation and lesions had recovered, as indicated by BALF biomarkers. No signs of lung fibrosis were observed. These results are consistent with previously reported typical change patterns of lung tissue in OA-induced lung injury models.[11−13]

SFN and SP-D Expression in BALF and Serum

We previously observed increases in SFN in BALF and serum of patients with DAD.[2,3] Therefore, we first investigated whether SFN levels are also changed in the BALF and serum of OA-induced ARDS rats. ELISA revealed that BALF SFN levels increased at 3 h after OA administration, peaked at 6 h, and then temporarily declined before increasing again at 48 h (Figure 3A). To examine whether the elevated SFN levels in BALF originate from blood or lung tissue, the ratios of SFN levels to ALB concentrations were compared in serum and BALF. If BALF SFN originated from the blood, the SFN/ALB ratio in BALF would be the same as that in serum. Notably, the SFN/ALB ratio in BALF at 3 to 144 h was significantly higher than that in serum, suggesting that SFN is released from the lung tissue into BALF (Table 1).

The serum SFN concentration ranged between approximately 9 and 18 ng/mL up to 48 h after OA administration (Figure 3B, Table 1), which is significantly higher than the normal levels in humans (below 0.5 ng/mL).[3] It is possible that there is a difference between humans and rats in the amount of SFN leaking into the circulating blood from epithelium of other tissues (e.g., abundant SFN-expressing tissues such as the skin and esophagus). However, serum SFN levels were markedly elevated by 96 h, which was a delayed response to the changes in SFN observed in BALF. In contrast, SP-D, a known marker of pulmonary fibrosis,[14] was increased in BALF between 24 and 48 h (Figure 3C), whereas only slight changes were found in serum

https://doi.org/10.1021/acs.jproteome.4c00980
J. Proteome Res. 2025, 24, 1941−1955

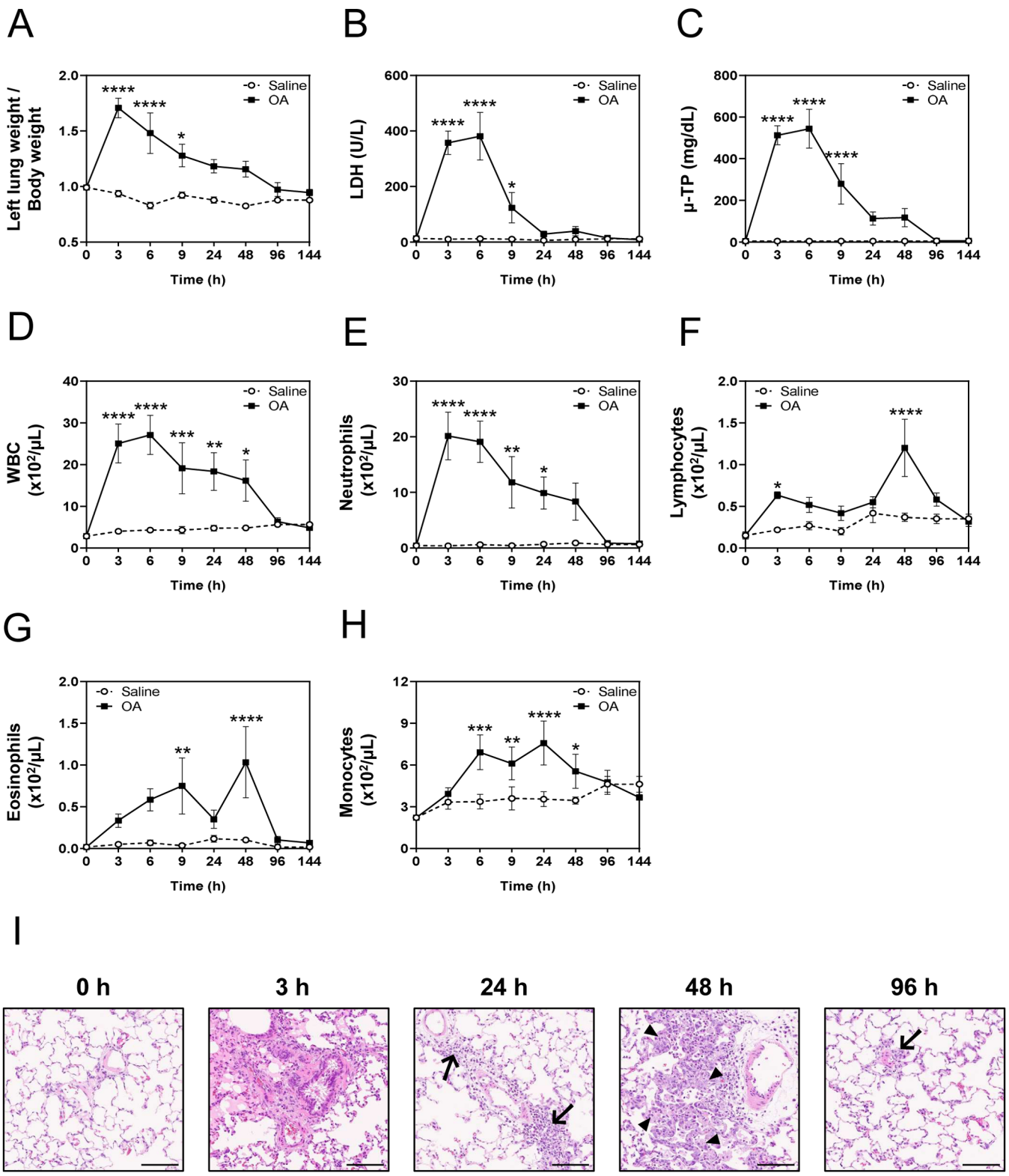

Figure 2. Characterization of lung injury in OA-induced ARDS rats. At the indicated time point after the injection of OA or saline, the lung tissues and BALF were subjected to the following tests: lung weight/body weight ratio assessment (A), and measurement of typical BALF biomarkers: LDH (B), μ-TP (C), WBC (D), neutrophils (E), lymphocytes (F), eosinophils (G), and monocytes (H). Data for the OA and saline groups are represented by black squares and white circles, respectively. Data are shown as mean ± SEM (n = 5 or 6). *p < 0.05, **p < 0.01, ***p < 0.001, ****p < 0.0001 vs the pretreated group (0 h) using two-way ANOVA and Bonferroni's posthoc test. (I) Representative histopathological findings in the lung tissues of OA-treated rats (hematoxylin and eosin staining). Arrows indicate infiltration of inflammatory cells. Arrowheads indicate hyperplasia of ATII cells. Scale bars = 100 μm.

https://doi.org/10.1021/acs.jproteome.4c00980
J. Proteome Res. 2025, 24, 1941−1955

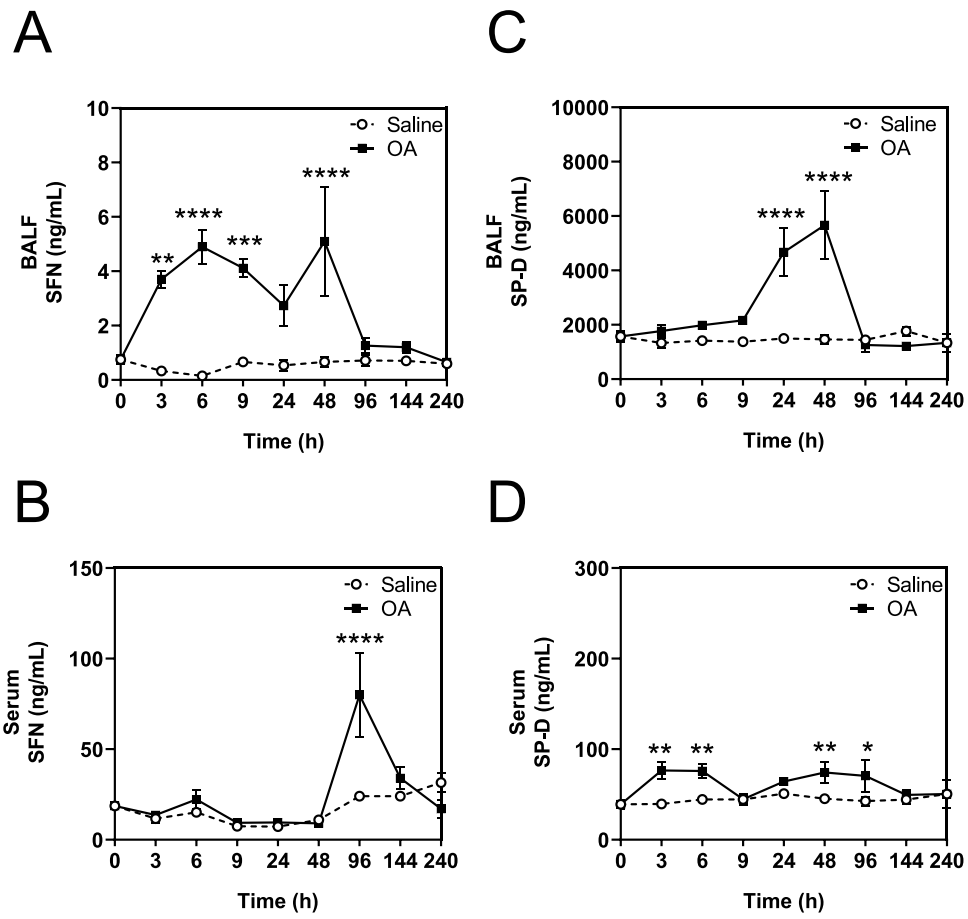

Figure 3. Time-dependent changes of SFN and SP-D levels in BALF and serum. SFN (A, B) and SP-D (C, D) levels were measured using ELISA. Biomarker levels in BALF (A, C) and serum (B, D) in the OA and saline groups are presented in black squares and white circles, respectively. Data are shown as mean ± SEM (n = 5 or 6). *p < 0.05, **p < 0.01, ***p < 0.001, ****p < 0.0001 vs 0 h using two-way ANOVA and Bonferroni's posthoc test.

Table 1. SFN and ALB Concentrations and Their Ratio in Serum and BALF Samples[a]

	BALF			serum			
time (h)	SFN (ng/mL)	ALB (mg/mL)	SFN/ALB (ng/mg)	SFN (ng/mL)	ALB (mg/mL)	SFN/ALB (ng/mg)	p-value
0	0.7 ± 0.4	0.03 ± 0.01	27.8 ± 12.2	18.6 ± 5.2	31.1 ± 3.0	0.6 ± 0.2	
3	3.7 ± 0.7	4.38 ± 0.54	0.9 ± 0.2	13.6 ± 3.5	32.8 ± 3.1	0.4 ± 0.1	0.004**
6	4.9 ± 1.4	4.41 ± 1.14	1.2 ± 0.3	22.2 ± 11.9	32.7 ± 3.2	0.7 ± 0.3	0.041*
9	4.1 ± 0.7	2.91 ± 1.90	2.1 ± 1.2	9.4 ± 3.5	36.0 ± 3.9	0.3 ± 0.1	0.002**
24	2.8 ± 1.7	1.14 ± 0.67	2.4 ± 0.9	9.5 ± 3.8	35.6 ± 5.5	0.3 ± 0.1	0.002**
48	5.1 ± 4.5	0.71 ± 0.51	9.4 ± 8.1	9.1 ± 4.4	35.1 ± 2.4	0.3 ± 0.1	0.002**
96	1.3 ± 0.6	0.03 ± 0.01	42.7 ± 23.8	80.0 ± 46.0	35.2 ± 4.6	2.2 ± 1.2	0.008**
144	1.2 ± 0.5	0.02 ± 0.00	50.1 ± 22.4	34.0 ± 14.2	35.1 ± 4.5	1.0 ± 0.4	0.002**
240	0.7 ± 0.1	0.03 ± 0.00	21.0 ± 1.4	17.0 ± 5.0	35.0 ± 4.1	0.5 ± 0.1	0.333

[a]Concentrations of SFN and ALB in lung tissues of OA-treated rats were quantified using ELISA analysis. Data are shown as mean ± SD (n = 5−6). *p 0.05, **p < 0.01, BALF SFN/ALB vs. serum SFN/ALB using the Welch's t-test.

(Figure 3D). This result shows that SFN is a biomarker with unique characteristics, distinct from that of SP-D.

Proteomic Analysis of Lung Tissue Extracts

We performed a proteomic analysis of lung tissues from OA-induced ARDS rats to investigate the mechanisms underlying the expression of SFN and its release into BALF and serum. Three individuals were randomly selected from each group at the following time points: 0 (pretreatment), 3, 6, 24, and 48 h. By using the DIA-MS method, over 9,100 protein groups were identified and quantified from each sample (Figure 4A). Subsequently, we identified several differentially expressed proteins in the OA groups. When applying a threshold of $\log_2$ [fold change] > 1.0 or < − 1.0 and p < 0.05 using the Welch's t test compared with the pretreated group based on the DIA-MS data, we found that the number of proteins with elevated expression was greater than the number of proteins with decreased expression after injecting OA. A total of 325, 192, 355, and 39 proteins were significantly increased at 3, 24, 48, and 96 h, respectively (Figure 4B).

https://doi.org/10.1021/acs.jproteome.4c00980
J. Proteome Res. 2025, 24, 1941−1955

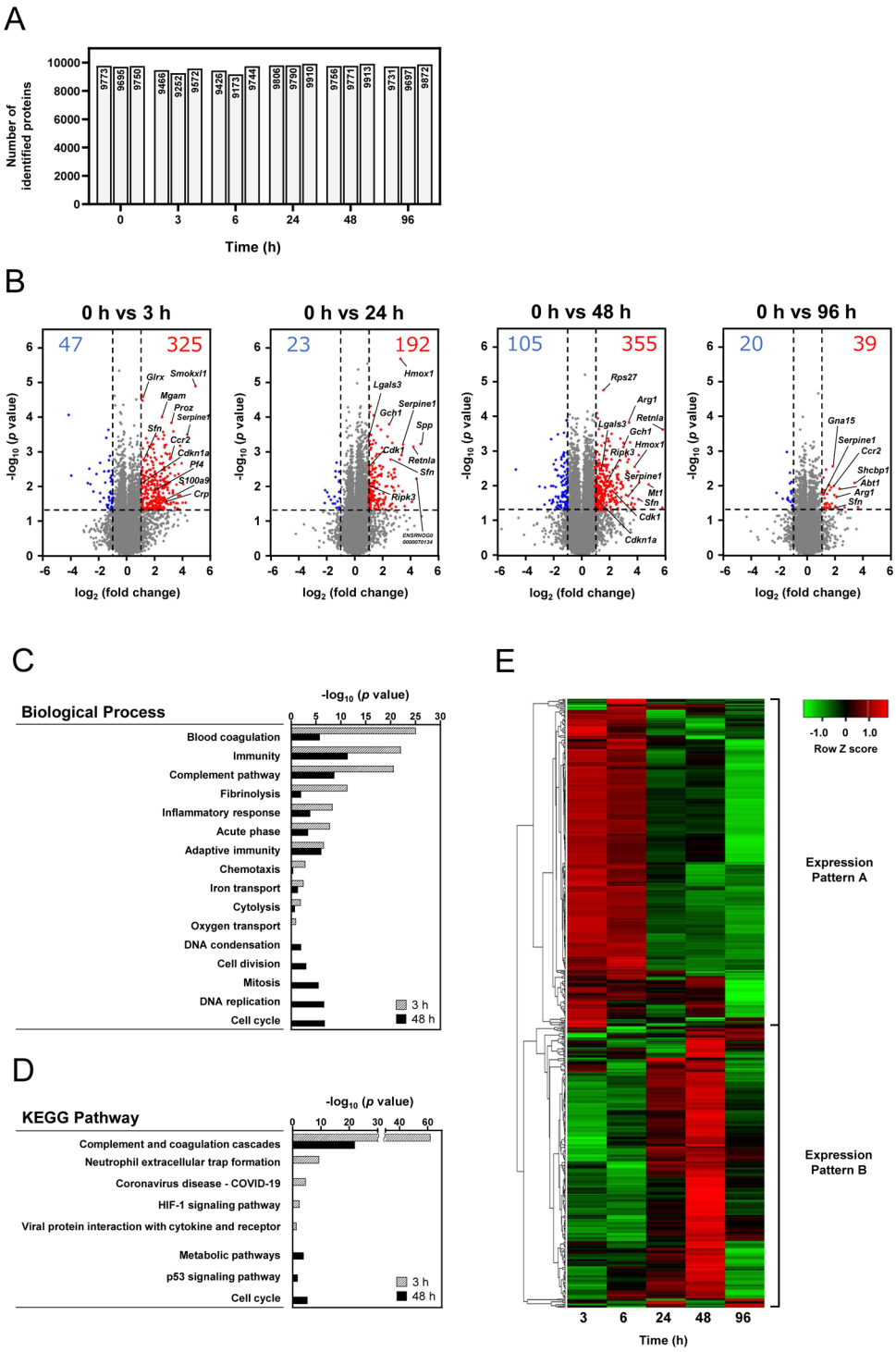

Figure 4. Proteomic analysis of lung tissue extracts in OA-induced ARDS rats. (A) Numbers of protein groups identified in the proteome analysis. (B) Volcano plots of differential proteins in the OA-treated rats. Red or blue dots indicate proteins with $\log_2$ fold change > 1.0 or < − 1.0, respectively, and p-value < 0.05 using Welch's t test compared with the pretreated group (0 h) (n = 3). A total of 325 proteins at 3 h, 192 proteins at 24 h, 355 proteins at 48 h, and 39 proteins at 96 h after OA administration were significantly increased. Conversely, significant decreases were observed in 47 proteins at 3 h, 23 proteins at 24 h, 105 proteins at 48 h, and 20 proteins at 96 h after OA administration. (C, D) Functional analysis of significantly elevated proteins at 3 (325 proteins) and 48 (355 proteins) h after OA administration. (C) Biological process category, (D) KEGG pathway category. (E) Heatmap and hierarchical clustering representing Pearson correlation. The heatmap illustrates the changes in expression levels of the 604 proteins that were significantly increased at 3, 6, 24, 48, and 96 h. Samples are given in the columns, and proteins are given in the rows. High expression is shown in red, and low expression is shown in green.

https://doi.org/10.1021/acs.jproteome.4c00980
J. Proteome Res. 2025, 24, 1941−1955

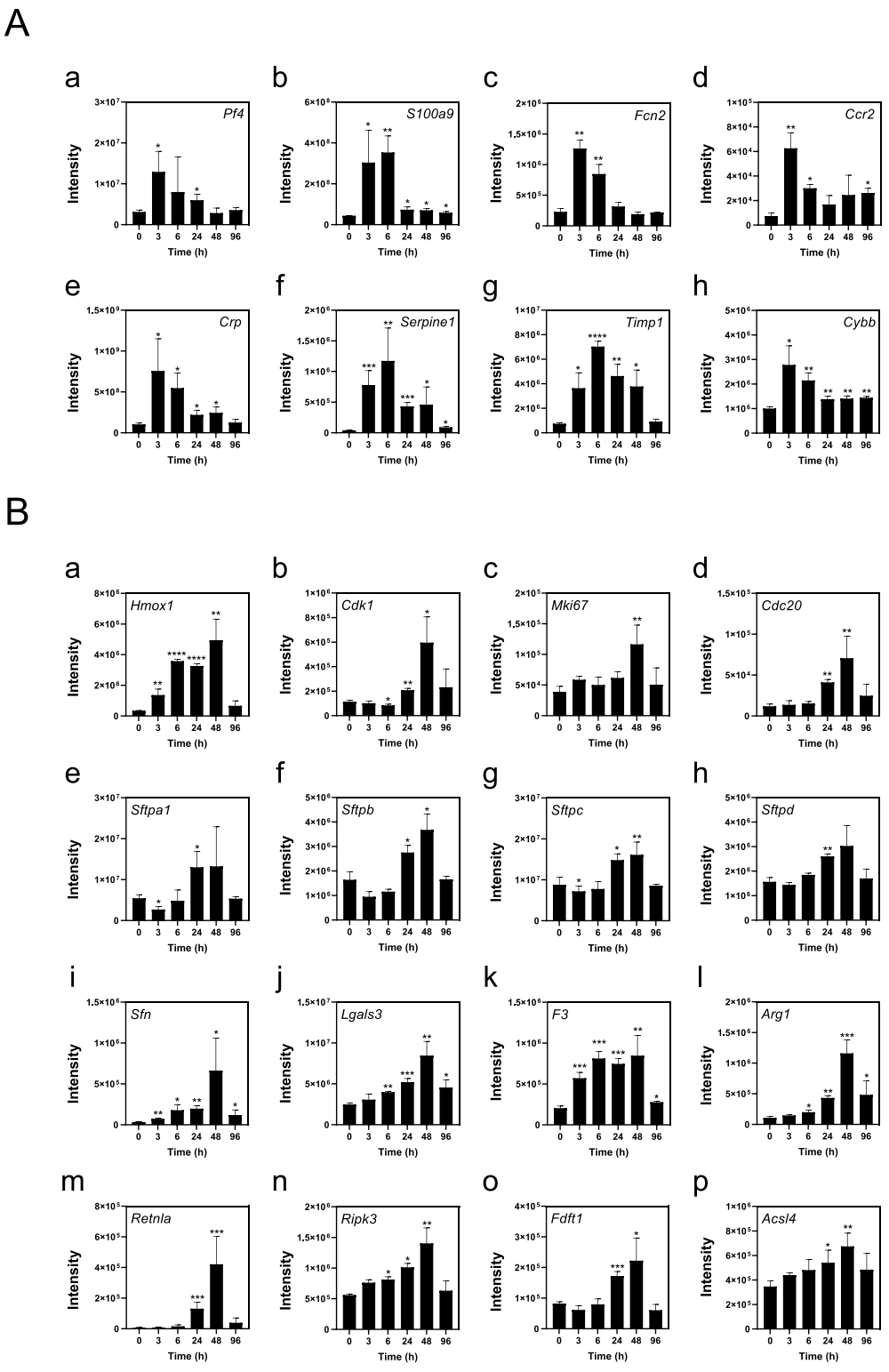

Figure 5. Representative proteins differentially expressed in lung tissues of OA-induced ARDS rats. (A) Proteins with the expression pattern A related to immunity and inflammatory response (a–e), and the HIF-1 signaling pathway (f–h). (B) Proteins with the expression pattern B related to the HIF-1 signaling pathway (a), cell cycle acceleration (b–d), surfactant proteins (e–h), SFN and PATS markers (i–k), tissue repair (i, m), and programmed cell death (a, n–p). Each protein is indicated by its official gene symbol. Intensities are indicated as quantification values obtained from proteomic analysis using DIA-NN and Perseus software. Data are shown as mean ± SEM ($n = 3$). *$p < 0.05$, **$p < 0.01$, ***$p < 0.001$, ***$p < 0.0001$ vs 0 h using the Welch's t test.

https://doi.org/10.1021/acs.jproteome.4c00980
J. Proteome Res. 2025, 24, 1941−1955

Table 2. Proteins Identified in Proteomic Analysis and Their Association with Lung Injury[a]

Uniprot#	protein	gene	pathway	association with lung injury	reference
expression pattern A					
P06765	platelet factor 4 (PF-4)	*Pf4*	immunity, chemotaxis	promotes ALI and fibrosis	17,18
P50116	protein S100-A9	*S100a9*	immunity, chemotaxis	promotes lung injury	19
P57756	ficolin-2	*Fcn2*	immunity	promotes lung injury, elevated in ARDS	20
O55193	C−C motif chemokine receptor 2 (CCR2)	*Ccr2i*	nflammatory response	promotes lung injury, elevated in severe COVID-19	21
P48199	C-reactive protein (CRP)	*Crp*	inflammatory response	inflammatory marker, elevated in severe COVID-19	24
P20961	plasminogen activator inhibitor-1 (PAI-1)	*Serpine1*	HIF-1 and p53 signaling	promotes fibrosis, elevated in severe COVID-19	25,26
P30120	TIMP metallopeptidase inhibitor-1 (TIMP-1)	*Timp1*	HIF-1 signaling	promotes immune response, elevated in ALI/ARDS	31
Q9ERL1	NADPH oxidase 2 (NOX2)	*Cybb*	HIF-1 signaling, Ferroptosis	promotes lung injury	33
expression pattern B					
P39951	cyclin-dependent kinase 1 (CDK1)	*Cdk1*	cell cycle acceleration	elevated in proliferating ATII	8
D4A0Y6	proliferation marker protein Ki67	*Mki67*	cell cycle acceleration	elevated in proliferating ATII, DAD/ARDS	8,43
Q62623	cell division cycle 20 (CDC20)	*Cdc20*	cell cycle acceleration	elevated in proliferating ATII	8
P08427	surfactant protein A1 (SP-A)	*Sftpa1*	biological regulation	expresses in ATII, elevated in ARDS	8,43
P22355	surfactant protein C (SP-B)	*Sftpb*	biological regulation	expresses in ATII	44
P11685	surfactant protein C (SP-C)	*Sftpc*	biological regulation	expresses in ATII	8
P35248	surfactant protein D (SP-D)	*Sftpd*	biological regulation	elevated in AT II, elevated in ARDS	44,45
Q5EBB0	stratifin	*Sfn*	cell cycle arrest, p53 signaling	elevated in PATS, severe COVID-19, DAD/ALI	2−4,7
P08699	galectin-3	*Lgals3*	immunity	elevated in PATS, severe COVID-19, IPF	7,46,47
P42533	tissue factor	*F3*	immunity	elevated in PATS, severe COVID-19	7,48
P07824	arginase-1	*Arg1*	immunity, metabolic pathway	promotes injured lung tissue repair	35
Q99P85	resistin-like α	*Retnla*	immunity	promotes injured lung tissue repair	35,36
Q9Z2P5	receptor-interacting serine-threonine kinase 3 (RIPK3)	*Ripk3*	necroptosis	promoting necroptosis, elevated in severe COVID-19, ALI/ARDS	37,38
P06762	heme oxygenase 1 (HO-1)	*Hmox1*	ferroptosis, HIF-1 signaling	regulating ferroptosis, reduces inflammation	34,39
Q02769	squalene synthase	*Fdft1*	ferroptosis, metabolic pathway	regulating ferroptosis, reduces inflammation	40,41
O35547	acyl-CoA synthetase long-chain family member 4 (ACSL4)	*Acsl4*	ferroptosis	regulating ferroptosis, elevated in ALI	42

[a]For each expression pattern, the Uniprot accession number, protein, gene, pathway, association with lung injury, and its reference are listed. Abbreviations; HIF-1, hypoxia-inducible factor-1; ALI, acute lung injury; ARDS, acute respiratory distress syndrome; IPF, idiopathic pulmonary fibrosis; DAD, diffuse alveolar damage; ATII, alveolar type-II cells; PATS, prealveolar type-I transitional cell state.

Proteome Signatures and Signaling Pathways in OA-Induced ARDS Rats

Next, we performed the gene ontology (GO) and Kyoto Encyclopedia of Genes and Genomes (KEGG) pathway analyses with a focus on the time points of 3 and 48 h, and found that many proteins showed increased expression (Figure 4C and D). The analyses revealed that the proteins increased at 3 h were significantly enriched in biological processes involved in "immunity," "blood coagulation," "COVID disease," and "HIF-1 signaling." In contrast, proteins increased at 48 h were characterized by the processes "cell cycle," "cell division," "p53 signaling," and "metabolic pathway." The hierarchical cluster analysis also clearly showed that the protein expression was classified into two patterns, peaking at approximately 3 h (pattern A) and 48 h (pattern B) (Figure 4E). SFN has functional annotations of the "p53 signaling pathway" and "cell cycle" and is included in the pattern B group.

Figure 5A and B show representative proteins with expression patterns A and B, respectively. Table 2 summarizes their attributed pathways and reports relevant to lung injury. Acute lung injury involves damage to the alveolar−capillary barrier, infiltration of inflammatory cells, and release of pro-inflammatory mediators, leading to inflammation and edema.[15,16] After the initial injury, repair mechanisms are activated, initiating the proliferation of ATII cells. These cells then undergo partial dedifferentiation and transition into prealveolar type-I transitional cell state (PATS) before differentiating into ATI cells, thereby restoring the alveolar surface and maintaining lung function.[9] Our proteomics data allowed us to observe this series of processes associated with tissue remodeling after lung injury.

The pattern A group included proteins associated with immune and inflammatory processes during acute lung injury (platelet factor 4 (PF-4, *Pf4*), protein S100-A9 (*S100a9*), ficolin-2 (*Fcn2*), C−C motif chemokine receptor 2 (*Ccr2*), and C-reactive protein (*Crp*)) (Figure 5A a−e). These proteins have been reported to contribute to acute lung injury progression by influencing inflammatory responses, immune cell recruitment, and alveolar-capillary barrier function.[17−24] Hypoxia-inducible factor (HIF)-1 signaling-related proteins plasminogen activator inhibitor-1 (PAI-1, *Serpine1*), TIMP metallopeptidase inhibitor-1 (TIMP-1, *Timp1*), and NADPH oxidase 2 (NOX2, *Cybb*) were also elevated with the expression pattern A (Figure 5A f−h). Although categorized into pattern B, heme oxygenase 1 (HO-1, *Hmox1*) is also related to the HIF-1 signaling and significantly increased at 3 h after OA treatment (Figure 5B a). These HIF-1 signaling-related proteins are thought to be involved in tissue hypoxic response, and to contribute to acute lung injury progression by regulating inflammation, oxidative stress, and alveolar-capillary barrier disruption.[25−34]

https://doi.org/10.1021/acs.jproteome.4c00980
J. Proteome Res. 2025, 24, 1941−1955

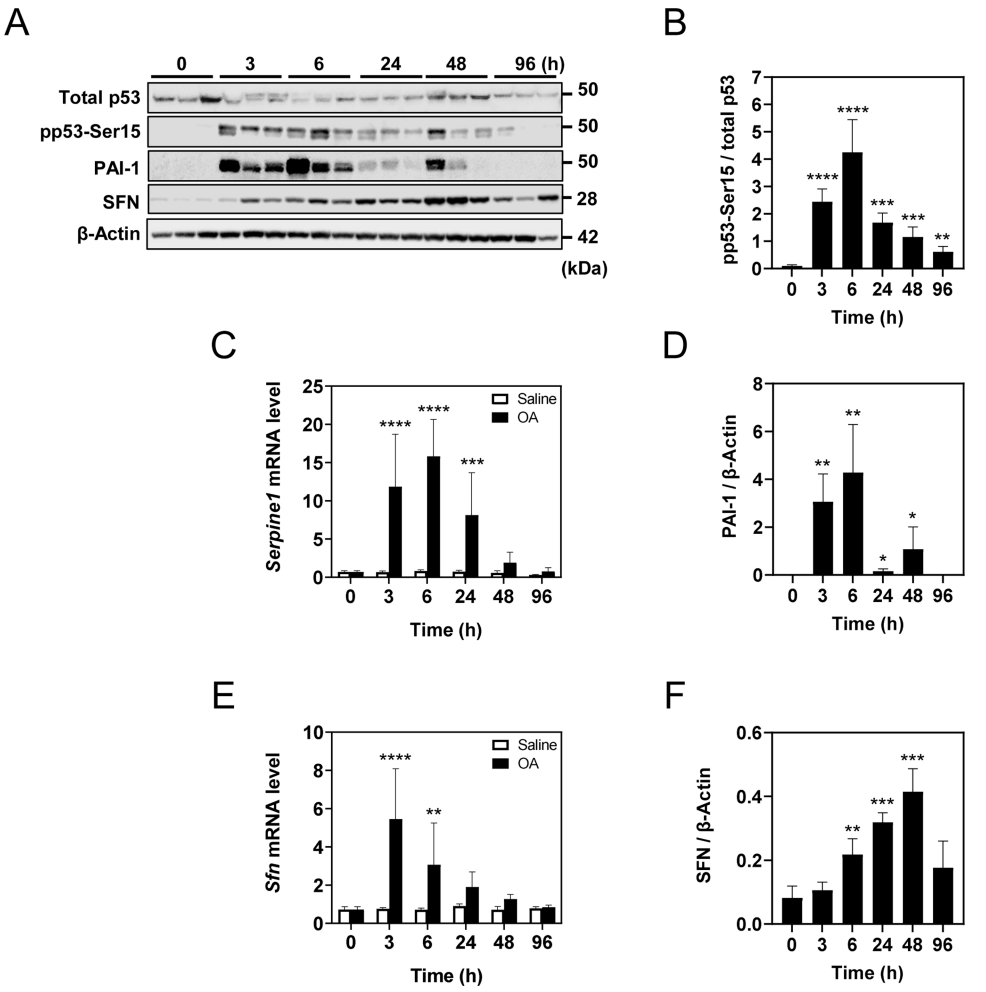

Figure 6. Western blotting and qRT-PCR analyses of PAI-1, SFN, and p53. (A) Representative Western blot images of the abundance of PAI-1, SFN, and p53-related proteins in the lung tissue extracts from OA-treated rats. (B, D, F) Graphs depicting the quantitation of phosphorylated p53 at Ser15 (pp53-Ser15, B), PAI-1 (*Serpine1*, D), and SFN (F) by ImageJ software. The abundance of pp53-Ser15 was normalized with that of total p53, and the abundance values of PAI-1 and SFN were normalized with that of β-actin. Data are shown as mean ± SEM ($n = 3$), $^{*}p < 0.05$, $^{**}p < 0.01$, $^{***}p < 0.001$, $^{****}p < 0.0001$ vs 0 h using one-way ANOVA and Dunnett's posthoc test. (C, E) mRNA levels of PAI-1 (*Serpine1*, C) and SFN (*Sfn*, E) in lung tissues of OA-treated rats. mRNA levels were quantified using qRT-PCR and normalized with those of *Tbp*. Data are shown as mean ± SEM ($n = 5$ or 6). $^{***}p < 0.001$, $^{****}p < 0.0001$ vs 0 h using two-way ANOVA and Bonferroni's posthoc test.

The pattern B group included cell cycle markers (cyclin-dependent kinase 1 (*Cdk1*), proliferation marker protein Ki67 (*Mki67*), and cell division cycle 20 (*Cdc20*)), which relate to cell-cycle acceleration (Figure 5B b–d), indicating that ATII cells proliferating, as evidenced by the increased expression of surfactant proteins (SP-A to -D, *Sftpa1*, *Sftpb*, *Sftpc*, and *Sftpd*, Figure 5B e–h), which are constitutively expressed in ATII cells. Simultaneously, SFN, which functions in cell cycle arrest via p53 signaling, was also elevated with the above cell cycle markers Figure 5B (i). Recently, p53 activation and SFN expression were reported to be upregulated in ATII cells in PATS, in association with the differentiation of ATII to ATI cells.[7] In addition, along with SFN expression, the expressions of galectin-3 (*Lgals3*) and tissue factor (*F3*), which have also been suggested to be PATS markers,[7] were also increased with the pattern B (Figure 5B j and k). These results suggest that both proliferating ATII cells and ATII cells in PATS are present in lung tissue after 48 h of OA treatment. This finding is supported by the increased expressions of two other PATS markers, p21 (*Cdkn1a*) and cellular communication network factor 2 (CCN2, *Ctgf*) (Supplementary Figure S1), although no significant changes were observed in the keratins *Krt7*, *Krt8*, *Krt17* and *Krt19*, which have been reported to be PATS markers[7] (Supplementary Figure S2). Tissue repair-related proteins (arginase-1 (*Arg1*) and resistin-like α (*Retnla*)) that were specifically produced by alveolar macrophages were also elevated (Figure 5B l and m), suggesting that the lung tissues at 48 h after OA treatment are undergoing a repair process.[35,36] On the other hand, proteins related to programmed cell death were also elevated. Receptor-interacting serine-threonine kinase 3 (*Ripk3*) induces necroptosis. Heme oxygenase 1 (HO-1, *Hmox1*), squalene synthase (*Fdft1*), and acyl-CoA synthetase long-chain family member 4 (*Acsl4*) induce ferroptosis (Figure 5B a,n–p). These proteins are involved in tissue repair via cell death.[34,37−42] Taken together, these experiments showed that proteins in the pattern B group contributed to several tissue remodeling processes involved in tissue repair and regeneration, including ATII proliferation and ATII− ATI differentiation.

Activation of p53 and Expression of SFN and PAI-1

The gene expression of SFN is known to be directly regulated by p53.[49] In this study, among the proteins related to the p53 signaling pathway that were found to be increased, PAI-1

https://doi.org/10.1021/acs.jproteome.4c00980
J. Proteome Res. 2025, 24, 1941−1955

(*Serpine1*) is a direct transcriptional target of p53.[50,51] Moreover, increased PAI-1 may activate p53.[27,52] p53 has been reported to promote ATI differentiation after lung injury.[8] As it was not possible to quantitatively evaluate p53 in the proteomic analysis due to a lack of stable MS-based detection, we compared and verified the expression of p53 with those of PAI-1 and SFN using Western blot analysis (Figure 6). No quantitative changes in total p53 were observed; however, its phosphorylated form at Ser15, indicative of p53 activation, was upregulated at 3 h after OA administration, peaked at 6 h, and then gradually decreased (Figure 6A, B). The variation patterns of the mRNA and protein levels of PAI-1, which were consistent with the results of the proteomic analysis (Figure 5A f), were remarkably similar to those of phospho-p53 (Ser15) (Figure 6C, D). *Sfn* mRNA showed a marked increase from 3 to 6 h, similar to the pattern of variation in phospho-p53 (Figure 6B, E), while SFN protein levels increased continuously to a peak at 48 h (Figure 6F), in agreement with the proteomic analysis (Figure 5B i). This difference in the pattern of upregulation of mRNA and protein for SFN suggests that its expression may be affected by p53 activation and post-transcriptional regulation. Additionally, another p53-target, p21 (*Cdkn1a*), also showed increased mRNA and protein levels at 6 and 48 h, supporting our finding of p53 activation in the OA group (Supplementary Figure S1A). These data suggest that activation of p53 signaling pathway is suggested to be occurred 3 to 6 h after OA administration.

SFN Expression in Proliferated ATII Cells

Figure 7 shows the results of the immunohistochemical analysis for SFN and for Ki67, a marker of ATII cell proliferation. At 3 h after OA administration, although few SFN-positive cells were observed, the appearance of Ki67-positive alveolar epithelial cells was noted, suggesting that proliferation of ATII cells had already begun at this time point. Subsequently, SFN-positive and Ki67-positive cells increased in a time-dependent manner, and both were highest in number at 48 h. Importantly, however, the patterns of SFN-staining and Ki67-staining were not an exact match, with SFN-positive cells being observed in only a part of proliferated ATII cells. This result suggests that SFN expression is not simply a characteristic of proliferated ATII cells, but rather might occur in ATII cells that are transitioning into the differentiation stage of ATI cells.

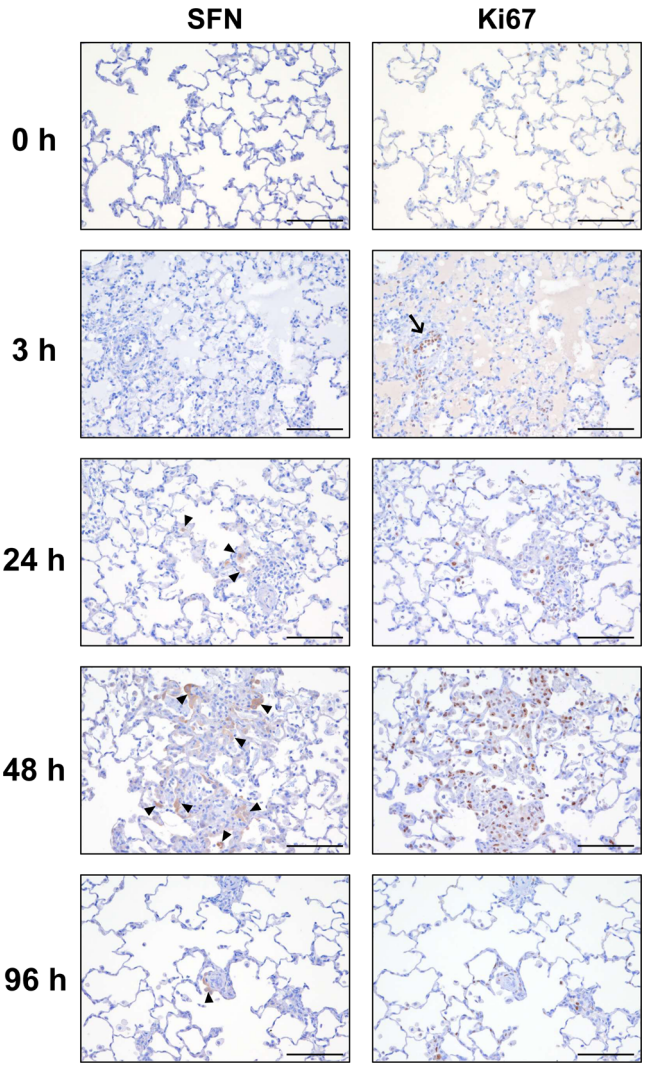

Figure 7. Immunohistochemical analysis of SFN and Ki67. Representative immunohistochemical findings for SFN and Ki67 in the lung tissues of OA-treated rats. An arrow marks the appearance of Ki67-positive ATII cells at 3 h after OA administration. Arrowheads indicate SFN-positive cells. Scale bars = 100 μm.

DISCUSSION

We investigated SFN expression in lung tissue and its release into BALF and serum using an OA-induced ARDS rat model. This study revealed the temporal aspects of SFN expression and release from lung cells during DAD progression, and SFN was upregulated in proliferated ATII cells during lung repair, in association with p53 and HIF-1 signaling essential for ATII-ATI differentiation. Our findings lead to understand previously unknown direct relationship between DAD pathology and SFN expression.

Although the details of the pathogenesis of OA-induced acute lung injury remain unclear, direct injury to the vascular endothelium and alveolar epithelium by OA is believed to be the primary cause.[12,13] Among the animal models of acute lung injury, the OA model exhibits pathological features such as tissue necrosis, edema, ATII cell proliferation, and fibrosis, which are similar to the features of human DAD.[11] Therefore, we used this animal model as a DAD/ARDS model in this study. DAD progresses through three phases: exudative, proliferative, and fibrotic.[15,16] In the exudative phase, inflammatory cells, such as neutrophils, infiltrate the alveolar space, damaging ATI epithelial and endothelial cells. The proliferative phase is characterized by the proliferation of ATII cells along the alveolar septa, often accompanied by metaplastic squamous epithelium. In the OA model used in this study, edema and hemorrhagic changes were observed throughout the lung tissue at 3 h. By 48 h, hyperplasia of ATII cells appeared in some lung tissues. The inflammatory response and epithelial cell proliferation subsided by 96 h, and no signs of pulmonary fibrosis were observed. These findings are typical responses observed in OA models, and are in accord with previous reports.[11−13,53] We also found that the OA model demonstrated SFN expression in proliferated ATII cells. This is in line with our previous experiments in human DAD autopsy specimens, which showed that SFN tended to be expressed in cells exhibiting ATII cell hyperplasia and squamous metaplasia.[3] However, such immunohistochemical analysis alone cannot definitively confirm that these epithelial cells are in a transitional state (PATS) that traverse between ATII and ATI cells. More refined and high-resolution investigations, such as single-cell analyses, are needed.

https://doi.org/10.1021/acs.jproteome.4c00980
J. Proteome Res. 2025, 24, 1941−1955

The elevation of SFN levels in the blood was delayed compared with the expression of SFN in BALF and lung tissues. The expression of SFN in tissue and BALF began to increase 3 h after OA administration, remained high until 48 h, then decreased at 96 h. In contrast, serum SFN was significantly elevated by 96 h. Since BALF is derived from alveolar fluid, which is closer to the tissue than blood, it is likely that SFN released from the alveolar epithelium reaches its peak earlier in BALF than in blood. Murata et al. have reported that in a rat model of bleomycin-induced lung injury, SP-D levels in BALF increased 3 days after bleomycin administration, followed by an increase in SP-D in serum 5 days later.[21,54] This SP-D behavior in the bleomycin model is similar to that of SFN in the OA model. However, unlike the bleomycin model, in which serum SP-D levels increased approximately 3-fold after lung injury,[54] they changed only slightly in the serum samples from our OA model, despite the marked elevation in BALF. As lung tissue fibrosis did not occur in our OA model, a marked increase in SP-D, a biomarker for lung fibrosis,[14] was likely not observed in serum.

In addition, SP-D (43 kDa) forms a dodecamer of approximately 500 kDa in alveolar fluid,[55,56] which is obviously larger than SFN (28 kDa). This difference in molecular size is likely to facilitate its transition from the alveoli into the bloodstream. Furthermore, since SP-D is a glycoprotein while SFN is not, differences in affinity for phospholipids and extracellular matrix components are likely, which may also result in varying efficiencies in crossing the air−blood barrier. Because of these different characteristics, the serum SFN level may reflect disruption of the air−blood barrier more rapidly than the serum SP-D level, even in the relatively early stages of pulmonary fibrosis before the disease progresses. Indeed, in our earlier study using serum samples from COVID-19 pneumonia patients, SFN was able to detect ARDS earlier than SP-D or KL-6.[2] These findings highlight the potential of SFN as a biomarker for DAD/ARDS, facilitating early detection and intervention before fibrosis develops. Although further validation is required to establish its clinical utility, but SFN may contribute to improved patient outcomes.

Although we previously demonstrated that p53-mediated apoptosis induces the extracellular release of SFN in vitro,[3] no significant changes were observed in the expression of apoptosis-inducing factors such as B-cell lymphoma 2-associated X protein (BAX), which is a direct transcriptional target of p53, in the OA model (Supplementary Table S1 and S2). Additionally, the GO and KEGG pathway analyses did not reveal any significant relationships with apoptotic functions. These findings suggest that apoptosis of alveolar epithelium is little induced in the OA model. In contrast, the expression pattern of RIPK3 resembled that of SFN (Figure 5B n and Table 2). RIPK3, a necroptosis-inducing protein, has also been suggested to be activated via interaction with SFN and to be involved in the process of lung tissue repair.[57] Moreover, proteins associated with ferroptosis, such as HO-1 and ACSL4, were also increased (Figure 5B a and p, Table 2). Increases in these ferroptosis-related proteins have also been observed in patients with ARDS.[42,58] It is possible that such cell death of ATII cells may have led to the extracellular release of SFN, ultimately resulting in increased serum SFN.

SFN is directly and transcriptionally regulated by the transcription factor p53. Thus, when SFN is upregulated, other p53 targets might also be upregulated. Through proteomic analysis, we revealed that one of the p53 targets, PAI-1 (gene *Serpine1*), which is a key regulator of plasminogen activators (tPA and uPA), is markedly increased in the OA model (Figures 5A f, 6C, D and Table 2). PAI-1 has multiple functions beyond inhibiting fibrinolysis, including regulating cell adhesion, migration, and proliferation. PAI-1 is expressed at higher levels in the lung tissue and plasma of patients with COVID-19 and DAD.[26,30] Although the precise mechanisms are unclear, PAI-1 has been reported to induce p21-dependent cellular senescence in injured ATII cells, thereby contributing to lung fibrosis.[27,29,52,59]

Additionally, PAI-1 is a transcriptional target of HIF-1α, a key factor in hypoxic signaling. In this study, the increases in proteins such as TIMP-1 and HO-1, which are also transcriptional targets of HIF-1α, occurred simultaneously (Figure 5A f, g and 5B a). All of these proteins are associated with acute lung injury and lung fibrosis. p53 activation is observed under hypoxic conditions. Hypoxia in particular is a common feature of ARDS, and it has been reported that hypoxic conditions induce HIF-1α.[60] Moreover, Rizou et al. showed that hypoxia induced SFN expression by binding HIF-1α to the promoter region of the *Sfn* gene in tubular epithelial cells in vivo and in vitro.[61] These findings led us to speculate that HIF-1 signaling is at least one of the cascades that might contribute to SFN expression in DAD progression. We are currently investigating the effects of these proteins on the upregulation of SFN in lung epithelial cells.

Lung tissue has a regenerative ability and initiates repair processes after acute injury. Alveoli, the functional units of the lungs, are mainly composed of ATI and ATII cells. Following lung injury, ATII cells proliferated and differentiate into ATI cells to restore the alveolar surface and maintain lung function.[7−9] Furthermore, several single-cell transcriptome analyses have observed transitional cells in "an intermediate state (named PATS)." These cells, which are in the process of differentiating from proliferating ATII cells into ATI cells, have also been described as "alveolar differentiation intermediates (ADI)," "damaged-associated transitional progenitors (DATPs)" or "AT0" cells.[7−9] It has been reported that the ATII cells in PATS require the activation of both p53 signaling and HIF-1 signaling pathways. In our OA rat model, the PATS markers (e.g., galectin-3 (*Lgals3*), tissue factor (*F3*), p21 (*Cdkn1a*), and CCN2 (*Ctgf*)) were increased (Figure 5B j, k, Table 2 and Supplementary Figure S1), with SFN showing increased expression accompanied by the activation of p53 signaling and an upregulation of HIF-1 signaling-related proteins (Figures 4D, 5A f−h and Table 2). These findings suggest that epithelial cell differentiation proceeded after lung injury in the OA-induced ARDS model and SFN is a biomarker closely associated with alveolar remodeling during this repair process.

Based on the findings of this study, the SFN release mechanism in the blood in acute lung injury can be deduced. In normal lungs, SFN expression level is low. After lung injury, as ATII cells proliferate, there is also an increase in ATII cells transitioning to PATS. In PATS, HIF-1 signaling and p53 signaling under hypoxic conditions are activated, leading to an increase in SFN gene expression and the accumulation of SFN protein. In DAD, the increased proliferation and cell death of ATII cells compared to other ILDs likely result in the release of SFN into the alveolar space and bloodstream.

The current study has some limitations. The OA model does not fully mimic the pathophysiology of human DAD/ARDS. The basal level of serum SFN in rats was approximately 9−18 ng/mL (Figure 3B and Table 1), which is significantly higher than the normal levels in humans (below 0.5 ng/mL).[3] ATII

https://doi.org/10.1021/acs.jproteome.4c00980
J. Proteome Res. 2025, 24, 1941−1955

cells begin to proliferate as early as 3 days (before the proliferation phase of DAD) following the onset of clinical ARDS.[53] Additionally, we previously observed that serum SFN levels were already elevated in the presevere stage of severe COVID-19 pneumonia.[2] However, the high basal level of rat SFN made it difficult to assess the early detectability of DAD using serum SFN in this rat model. Furthermore, acute lung injury induces hemorrhagic changes, resulting in blood contamination in BALF samples, particularly within 9 h after OA administration. Therefore, the amount of SFN released from the alveolar epithelium into BALF may not have been accurately assessed. As an alternative approach, we evaluated the increase of lung tissue−derived SFN by comparing the SFN/ALB ratio in BALF and serum samples (Table 1). Additionally, although our ARDS rat model with a single OA dose is a highly reproducible model for the acute and proliferative phases of human ARDS, unlike in human DAD/ARDS, our ARDS model rats recover without progressing to the fibrotic phase. Therefore, proteins involved in lung fibrosis, such as SP-D, could not be evaluated. In addition, we observed that SFN was produced in the tissue after lung injury, increased in BALF at 48 h, and reflected in the blood at 96 h (Figure 3A and B). However, the proteomic data in this study did not provide conclusive evidence connecting it to the mechanism and time course of SFN release into the blood. Moreover, the proteomic data were derived from total lysates of lung tissue, and as such, these data likely reflected the simultaneous detection of various biological responses across multiple cells types, including ATI and ATII cells, endothelial cells, macrophages, and fibroblasts; these responses would have included promotion and inhibition of cell proliferation, cell differentiation, cell repair, and cell death. To gain a more detailed understanding of the relationship between DAD and SFN, the differentiation from ATII to ATI and the mechanisms of SFN extracellular release, further analyses at the individual cell level will be required.

In this study, we aimed to clarify the role of SFN in the pathology of DAD-type ILD by comparing the pathological features of lung tissue and proteome changes using the OA-induced ARDS rat model. Our data suggest that SFN expression in proliferated ATII cells, accompanied by p53 activation, is essential for the differentiation into ATI cells. SFN may be a biomarker closely related to alveolar remodeling during the repair process after lung injury. To the best of our knowledge, this is the first report to examine temporal changes in the SFN expression in blood, BALF and tissues, in conjunction with proteomic data, using an ARDS animal model. These findings provide data not available in clinical studies and support the suitability of SFN as a biomarker for diagnosing DAD-type ILD.

■ ASSOCIATED CONTENT

Data Availability Statement

Mass spectrometry proteomics data have been deposited to the ProteomeXchange Consortium (PXD057386, http://www.proteomexchange.org/) via the jPOST partner repository (JPST003445, https://jpostdb.org/).

Supporting Information

The Supporting Information is available free of charge at https://pubs.acs.org/doi/10.1021/acs.jproteome.4c00980.

Table S1: Identified proteins (raw data) obtained from proteomic analysis using DIA-NN software; Table S2: Adjusted quantification values obtained from proteomic analysis using Perseus software (XLSX)

Figure S1: Protein and mRNA levels of p21 and CCN2; Figure S2: Proteins related to PATS; Figure S3: Western blotting images of the entire membrane (PDF)

■ AUTHOR INFORMATION

Corresponding Author

Noriaki Arakawa − *Division of Medicinal Safety Science, National Institute of Health Sciences, Kawasaki, Kanagawa 210-9501, Japan*; Phone: +81-44-270-6625; Email: arakawa@nihs.go.jp; Fax: +81-44-270-6627

Authors

Ayaka Yoshida − *Division of Medicinal Safety Science, National Institute of Health Sciences, Kawasaki, Kanagawa 210-9501, Japan*; orcid.org/0000-0002-6925-3562

Yuya Hashimoto − *Division of Medicinal Safety Science, National Institute of Health Sciences, Kawasaki, Kanagawa 210-9501, Japan*

Hirotoshi Akane − *Division of Pathology, National Institute of Health Sciences, Kawasaki, Kanagawa 210-9501, Japan*

Shinichiro Matsuyama − *Division of Medicinal Safety Science, National Institute of Health Sciences, Kawasaki, Kanagawa 210-9501, Japan*

Takeshi Toyoda − *Division of Pathology, National Institute of Health Sciences, Kawasaki, Kanagawa 210-9501, Japan*

Kumiko Ogawa − *Division of Pathology, National Institute of Health Sciences, Kawasaki, Kanagawa 210-9501, Japan*

Yoshiro Saito − *Division of Medicinal Safety Science, National Institute of Health Sciences, Kawasaki, Kanagawa 210-9501, Japan*

Ruri Kikura-Hanajiri − *Division of Medicinal Safety Science, National Institute of Health Sciences, Kawasaki, Kanagawa 210-9501, Japan*

Complete contact information is available at: https://pubs.acs.org/10.1021/acs.jproteome.4c00980

Author Contributions

Conceptualization, A.Y., N.A., and Y.S.; Experiments, A.Y., Y.H., H.A., T.T., S.M., K.O., and N.A.; Data analysis, A.Y., H.A., and N.A.; Funding acquisition, N.A. and Y.S.; Project administration, N.A. and Y.S.; Supervision, N.A. and R.H.; Writing original draft, A.Y. and N.A.; Final draft/editing, all authors.

Notes

The authors declare no competing financial interest.

■ ACKNOWLEDGMENTS

Financial support was received in the form of grants from the Japan Agency for Medical Research and Development (nos. 20mk0101173 and 23mk0121256 to N.A. and Y.S.), and a KAKENHI Grant-in-Aid for Scientific Research (C) from the Ministry of Education, Culture, Sports, Science and Technology of Japan, Science and Technology Agency (no. g20K07366 to N.A.). We thank Yoshiki Miyagi for his assistance.

■ ABBREVIATIONS

DAD, diffuse alveolar damage; ILD, interstitial lung disease; SFN, stratifin; OA, oleic acid; IPF, idiopathic pulmonary fibrosis; COVID-19, coronavirus disease 2019; ARDS, acute respiratory distress syndrome; DILD, drug-induced ILD; EGFR-TKIs, epidermal growth factor receptor-tyrosine kinase inhibitors; SP-D, surfactant protein D; KL-6, Krebs von den

https://doi.org/10.1021/acs.jproteome.4c00980
J. Proteome Res. 2025, 24, 1941−1955

Lungen-6; BALF, bronchoalveolar lavage fluid; LDH, lactate dehydrogenase; μ-TP, micrototal protein; DIA-MS, data-independent acquisition mass spectrometry; BSA, bovine serum albumin; Tbp, TATA box binding protein; ALB, albumin; ATI, alveolar type-I cells; ATII, alveolar type II cells; PATS, prealveolar type-I transitional cell state; PF-4, platelet factor 4; S100A9, protein S100-A9; FCN2, ficolin-2; CCR2, C−C motif chemokine receptor 2; CRP, C-reactive protein; HIF-1, hypoxia-inducible factor 1; PAI-1, plasminogen activator inhibitor-1; SERPINE1, serpin family E member 1; TIMP-1, TIMP metallopeptidase inhibitor-1; NOX2, NADPH oxidase 2; HO-1, heme oxygenase 1; CDK1, cyclin-dependent kinase 1; CDC20, cell division cycle 20; LGALS3, galectin-3; CCN2, cellular communication network factor 2; KRT, keratin; ARG1, arginase-1; RETNLA, resistin-like α; RIPK3, receptor-interacting serine-threonine kinase 3; ACSL4, acyl-CoA synthetase long-chain family member 4; BAX, B-cell lymphoma 2-asocciated X protein

REFERENCES

(1) Kawase, S.; Hattori, N.; Ishikawa, N.; Horimasu, Y.; Fujitaka, K.; Furonaka, O.; Isobe, T.; Miyoshi, S.; Hamada, H.; Yamane, T.; et al. Change in serum KL-6 level from baseline is useful for predicting life-threatening EGFR-TKIs induced interstitial lung disease. *Respir Res.* **2011**, *12* (1), 97.

(2) Arakawa, N.; Matsuyama, S.; Matsuoka, M.; Kitamura, I.; Miyashita, K.; Kitagawa, Y.; Imai, K.; Ogawa, K.; Maeda, T.; Saito, Y.; Hasegawa, C. Serum stratifin and presepsin as candidate biomarkers for early detection of COVID-19 disease progression. *J. Pharmacol Sci.* **2022**, *150* (1), 21−30.

(3) Arakawa, N.; Ushiki, A.; Abe, M.; Matsuyama, S.; Saito, Y.; Kashiwada, T.; Horimasu, Y.; Gemma, A.; Tatsumi, K.; Hattori, N.; et al. Stratifin as a novel diagnostic biomarker in serum for diffuse alveolar damage. *Nat. Commun.* **2022**, *13* (1), No. 5854.

(4) Sakuma, N.; Abe, M.; Ishii, D.; Kawasaki, T.; Arakawa, N.; Matsuyama, S.; Saito, Y.; Suzuki, T.; Tatsumi, K. Serum stratifin measurement is useful for evaluating disease severity and outcomes in patients with acute exacerbation of interstitial lung disease: a retrospective study. *BMC Pulm Med.* **2024**, *24* (1), 364.

(5) Dellambra, E.; Golisano, O.; Bondanza, S.; Siviero, E.; Lacal, P.; Molinari, M.; D'Atri, S.; De Luca, M. Downregulation of 14−3-3sigma prevents clonal evolution and leads to immortalization of primary human keratinocytes. *J. Cell Biol.* **2000**, *149* (5), 1117−1130.

(6) Taylor, W. R.; Stark, G. R. Regulation of the G2/M transition by p53. *Oncogene* **2001**, *20* (15), 1803−1815.

(7) Kobayashi, Y.; Tata, A.; Konkimalla, A.; Katsura, H.; Lee, R. F.; Ou, J.; Banovich, N. E.; Kropski, J. A.; Tata, P. R. Persistence of a regeneration-associated, transitional alveolar epithelial cell state in pulmonary fibrosis. *Nat. Cell Biol.* **2020**, *22* (8), 934−946.

(8) Choi, J.; Park, J. E.; Tsagkogeorga, G.; Yanagita, M.; Koo, B. K.; Han, N.; Lee, J. H. Inflammatory Signals Induce AT2 Cell-Derived Damage-Associated Transient Progenitors that Mediate Alveolar Regeneration. *Cell Stem Cell* **2020**, *27* (3), 366−382.E7.

(9) Chen, Y.; Li, Z.; Ji, G.; Wang, S.; Mo, C.; Ding, B. S. Lung regeneration: diverse cell types and the therapeutic potential. *MedComm* **2024**, *5* (2), No. e494.

(10) Kadam, A. H.; Schnitzer, J. E. Characterization of acute lung injury in the bleomycin rat model. *Physiol Rep.* **2023**, *11* (5), No. e15618.

(11) Wang, H. M.; Bodenstein, M.; Markstaller, K. Overview of the pathology of three widely used animal models of acute lung injury. *Eur. Surg Res.* **2008**, *40* (4), 305−316.

(12) Matute-Bello, G.; Frevert, C. W.; Martin, T. R. Animal models of acute lung injury. *Am. J. Physiol Lung Cell Mol. Physiol.* **2008**, *295* (3), L379−399.

(13) Gonçalves-de-Albuquerque, C. F.; Silva, A. R.; Burth, P.; Castro-Faria, M. V.; Castro-Faria-Neto, H. C. Acute Respiratory Distress Syndrome: Role of Oleic Acid-Triggered Lung Injury and Inflammation. *Mediators Inflamm* **2015**, *2015*, No. 260465.

(14) Tomos, I.; Roussis, I.; Matthaiou, A. M.; Dimakou, K. Molecular and Genetic Biomarkers in Idiopathic Pulmonary Fibrosis: Where Are We Now? *Biomedicines* **2023**, *11* (10), 2796.

(15) Leslie, K. O. My approach to interstitial lung disease using clinical, radiological and histopathological patterns. *J. Clin Pathol* **2009**, *62* (5), 387−401.

(16) Butt, Y.; Kurdowska, A.; Allen, T. C. Acute Lung Injury: A Clinical and Molecular Review. *Arch Pathol Lab Med.* **2016**, *140* (4), 345−350.

(17) Bdeir, K.; Gollomp, K.; Stasiak, M.; Mei, J.; Papiewska-Pajak, I.; Zhao, G.; Worthen, G. S.; Cines, D. B.; Poncz, M.; Kowalska, M. A. Platelet-Specific Chemokines Contribute to the Pathogenesis of Acute Lung Injury. *Am. J. Respir. Cell Mol. Biol.* **2017**, *56* (2), 261−270.

(18) Affandi, A. J.; Carvalheiro, T.; Ottria, A.; de Haan, J. J.; Brans, M. A. D.; Brandt, M. M.; Tieland, R. G.; Lopes, A. P.; Fernandez, B. M.; Bekker, C. P. J.; et al. CXCL4 drives fibrosis by promoting several key cellular and molecular processes. *Cell Rep.* **2022**, *38* (1), No. 110189.

(19) Zhao, B.; Lu, R.; Chen, J.; Xie, M.; Zhao, X.; Kong, L. S100A9 blockade prevents lipopolysaccharide-induced lung injury via suppressing the NLRP3 pathway. *Respir Res.* **2021**, *22* (1), 45.

(20) Huang, L.; Tan, X.; Xuan, W.; Luo, Q.; Xie, L.; Xi, Y.; Li, R.; Li, L.; Li, F.; Zhao, M.; et al. Ficolin-A/2 Aggravates Severe Lung Injury through Neutrophil Extracellular Traps Mediated by Gasdermin D-Induced Pyroptosis. *Am. J. Pathol.* **2024**, *194* (6), 989−1006.

(21) Files, D. C.; Tacke, F.; O'Sullivan, A.; Dorr, P.; Ferguson, W. G.; Powderly, W. G. Rationale of using the dual chemokine receptor CCR2/CCR5 inhibitor cenicriviroc for the treatment of COVID-19. *PLoS Pathog.* **2022**, *18* (6), No. e1010547.

(22) Oliveira, V. L. S. d.; Pollenus, E.; Berghmans, N.; Queiroz-Junior, C. M.; Blanter, M.; Mattos, M. S.; Teixeira, M. M.; Proost, P.; Van den Steen, P. E.; Amaral, F. A.; Struyf, S. Absence of CCR2 Promotes Proliferation of Alveolar Macrophages That Control Lung Inflammation in Acute Respiratory Distress Syndrome in Mice. *Int. J. Mol. Sci.* **2022**, *23* (21), 12920.

(23) Gutierrez-Chavez, C.; Aperrigue-Lira, S.; Ortiz-Saavedra, B.; Paz, I. Chemokine receptors in COVID-19 infection. *Int. Rev. Cell Mol. Biol.* **2024**, *388*, 53−94.

(24) Ponti, G.; Maccaferri, M.; Ruini, C.; Tomasi, A.; Ozben, T. Biomarkers associated with COVID-19 disease progression. *Crit Rev. Clin Lab Sci.* **2020**, *57* (6), 389−399.

(25) Matsuyama, T.; Kubli, S. P.; Yoshinaga, S. K.; Pfeffer, K.; Mak, T. W. An aberrant STAT pathway is central to COVID-19. *Cell Death Differ.* **2020**, *27* (12), 3209−3225.

(26) D'Agnillo, F.; Walters, K. A.; Xiao, Y.; Sheng, Z. M.; Scherler, K.; Park, J.; Gygli, S.; Rosas, L. A.; Sadtler, K.; Kalish, H.; et al. Lung epithelial and endothelial damage, loss of tissue repair, inhibition of fibrinolysis, and cellular senescence in fatal COVID-19. *Sci. Transl Med.* **2021**, *13* (620), No. eabj7790.

(27) Jiang, C.; Liu, G.; Luckhardt, T.; Antony, V.; Zhou, Y.; Carter, A. B.; Thannickal, V. J.; Liu, R. M. Serpine 1 induces alveolar type II cell senescence through activating p53-p21-Rb pathway in fibrotic lung disease. *Aging Cell* **2017**, *16* (5), 1114−1124.

(28) Osterholzer, J. J.; Christensen, P. J.; Lama, V.; Horowitz, J. C.; Hattori, N.; Subbotina, N.; Cunningham, A.; Lin, Y.; Murdock, B. J.; Morey, R. E.; et al. PAI-1 promotes the accumulation of exudate macrophages and worsens pulmonary fibrosis following type II alveolar epithelial cell injury. *J. Pathol* **2012**, *228* (2), 170−180.

(29) Adnot, S.; Breau, M.; Houssaini, A. PAI-1: A New Target for Controlling Lung-Cell Senescence and Fibrosis? *Am. J. Respir. Cell Mol. Biol.* **2020**, *62* (3), 271−272.

(30) Ackermann, M.; Verleden, S. E.; Kuehnel, M.; Haverich, A.; Welte, T.; Laenger, F.; Vanstapel, A.; Werlein, C.; Stark, H.; Tzankov, A.; et al. Pulmonary Vascular Endothelialitis, Thrombosis, and Angiogenesis in Covid-19. *N Engl J. Med.* **2020**, *383* (2), 120−128.

(31) Almuntashiri, S.; Alhumaid, A.; Zhu, Y.; Han, Y.; Dutta, S.; Khilji, O.; Zhang, D.; Wang, X. TIMP-1 and its potential diagnostic and

https://doi.org/10.1021/acs.jproteome.4c00980
J. Proteome Res. 2025, 24, 1941−1955

prognostic value in pulmonary diseases. *Chin Med. J. Pulm Crit Care Med.* **2023**, *1* (2), 67−76.
(32) Almuntashiri, S.; Jones, T. W.; Wang, X.; Sikora, A.; Zhang, D. Plasma TIMP-1 as a sex-specific biomarker for acute lung injury. *Biol. Sex Differ* **2022**, *13* (1), 70.
(33) Sul, O. J.; Ra, S. W. Quercetin Prevents LPS-Induced Oxidative Stress and Inflammation by Modulating NOX2/ROS/NF-kB in Lung Epithelial Cells. *Molecules* **2021**, *26* (22), 6949 DOI: 10.3390/molecules26226949.
(34) Li, X.; Yu, J.; Gong, L.; Zhang, Y.; Dong, S.; Shi, J.; Li, C.; Li, Y.; Zhang, Y.; Li, H. Heme oxygenase-1(HO-1) regulates Golgi stress and attenuates endotoxin-induced acute lung injury through hypoxia inducible factor-1alpha (HIF-1alpha)/HO-1 signaling pathway. *Free Radic Biol. Med.* **2021**, *165*, 243−253.
(35) Wang, Q.; Zhang, H. W.; Mei, H. X.; Ye, Y.; Xu, H. R.; Xiang, S. Y.; Yang, Q.; Zheng, S. X.; Smith, F. G.; Jin, S. W. MCTR1 enhances the resolution of lipopolysaccharide-induced lung injury through STAT6-mediated resident M2 alveolar macrophage polarization in mice. *J. Cell Mol. Med.* **2020**, *24* (17), 9646−9657.
(36) Lin, Q.; Johns, R. A. Resistin family proteins in pulmonary diseases. *Am. J. Physiol Lung Cell Mol. Physiol* **2020**, *319* (3), L422−L434.
(37) Dai, W.; Cheng, J.; Leng, X.; Hu, X.; Ao, Y. The potential role of necroptosis in clinical diseases (Review). *Int. J. Mol. Med.* **2021**, *47* (5), 89.
(38) Wang, L.; Zhou, L.; Zhou, Y.; Liu, L.; Jiang, W.; Zhang, H.; Liu, H. Necroptosis in Pulmonary Diseases: A New Therapeutic Target. *Front. Pharmacol.* **2021**, *12*, No. 737129.
(39) Chen, X.; Wang, Y.; Xie, X.; Chen, H.; Zhu, Q.; Ge, Z.; Wei, H.; Deng, J.; Xia, Z.; Lian, Q. Heme Oxygenase-1 Reduces Sepsis-Induced Endoplasmic Reticulum Stress and Acute Lung Injury. *Mediators Inflamm* **2018**, *2018*, No. 9413876.
(40) Picón, D. F.; Skouta, R. Unveiling the Therapeutic Potential of Squalene Synthase: Deciphering Its Biochemical Mechanism, Disease Implications, and Intriguing Ties to Ferroptosis. *Cancers* **2023**, *15* (14), 3731 DOI: 10.3390/cancers15143731.
(41) Pu, X.; Lin, X.; Qi, Y.; Li, Y.; Li, T.; Liu, Y.; Wei, D. Effects of Fdft 1 gene silencing and VD3 intervention on lung injury in hypoxia-stressed rats. *Genes Genomics* **2022**, *44* (10), 1201−1213.
(42) Yu, T.; Sun, S. Role and mechanism of ferroptosis in acute lung injury. *Cell Cycle* **2023**, *22* (19), 2119−2129.
(43) Kang, D.; Nakayama, T.; Togashi, M.; Yamamoto, M.; Takahashi, M.; Kunugi, S.; Ishizaki, M.; Fukuda, Y. Two forms of diffuse alveolar damage in the lungs of patients with acute respiratory distress syndrome. *Hum. Pathol.* **2009**, *40* (11), 1618−1627.
(44) Ghati, A.; Dam, P.; Tasdemir, D.; Kati, A.; Sellami, H.; Sezgin, G. C.; Ildiz, N.; Franco, O. L.; Mandal, A. K.; Ocsoy, I. Exogenous pulmonary surfactant: A review focused on adjunctive therapy for severe acute respiratory syndrome coronavirus 2 including SP-A and SP-D as added clinical marker. *Curr. Opin. Colloid Interface Sci.* **2021**, *51*, No. 101413.
(45) Shimada, I.; Kubota, A.; Katoh, M.; Suzuki, F. Hyperoxia causes diffuse alveolar damage through mechanisms involving upregulation of c-Myc/Bax and enhanced production of reactive oxygen species. *Respir. Investig.* **2016**, *54* (1), 59−68.
(46) Nikitopoulou, I.; Vassiliou, A. G.; Athanasiou, N.; Jahaj, E.; Akinosoglou, K.; Dimopoulou, I.; Orfanos, S. E.; Dimakopoulou, V.; Schinas, G.; Tzouvelekis, A.; et al. Increased Levels of Galectin-3 in Critical COVID-19. *Int. J. Mol. Sci.* **2023**, *24* (21), 15833.
(47) Mackinnon, A. C.; Gibbons, M. A.; Farnworth, S. L.; Leffler, H.; Nilsson, U. J.; Delaine, T.; Simpson, A. J.; Forbes, S. J.; Hirani, N.; Gauldie, J.; Sethi, T. Regulation of transforming growth factor-beta1-driven lung fibrosis by galectin-3. *Am. J. Respir Crit. Care Med.* **2012**, *185* (5), 537−546.
(48) Sachetto, A. T. A.; Mackman, N. Tissue Factor and COVID-19: An Update. *Curr. Drug Targets* **2022**, *23* (17), 1573−1577.
(49) Hermeking, H.; Lengauer, C.; Polyak, K.; He, T. C.; Zhang, L.; Thiagalingam, S.; Kinzler, K. W.; Vogelstein, B. 14−3-3sigma is a p53-regulated inhibitor of G2/M progression. *Mol. Cell* **1997**, *1* (1), 3−11.
(50) Kawarada, Y.; Inoue, Y.; Kawasaki, F.; Fukuura, K.; Sato, K.; Tanaka, T.; Itoh, Y.; Hayashi, H. TGF-beta induces p53/Smads complex formation in the PAI-1 promoter to activate transcription. *Sci. Rep* **2016**, *6*, No. 35483.
(51) Shetty, S. K.; Bhandary, Y. P.; Marudamuthu, A. S.; Abernathy, D.; Velusamy, T.; Starcher, B.; Shetty, S. Regulation of airway and alveolar epithelial cell apoptosis by p53-Induced plasminogen activator inhibitor-1 during cigarette smoke exposure injury. *Am. J. Respir. Cell Mol. Biol.* **2012**, *47* (4), 474−483.
(52) Rana, T.; Jiang, C.; Banerjee, S.; Yi, N.; Zmijewski, J. W.; Liu, G.; Liu, R. M. PAI-1 Regulation of p53 Expression and Senescence in Type II Alveolar Epithelial Cells. *Cells* **2023**, *12* (15), 2008.
(53) Tomashefski, J. F., Jr. Pulmonary pathology of acute respiratory distress syndrome. *Clin Chest Med.* **2000**, *21* (3), 435−466.
(54) Murata, M.; Otsuka, M.; Ashida, N.; Yamada, G.; Kuronuma, K.; Chiba, H.; Takahashi, H. Surfactant protein D is a useful biomarker for monitoring acute lung injury in rats. *Exp. Lung Res.* **2016**, *42* (6), 314−321.
(55) Zhang, L.; Ikegami, M.; Crouch, E. C.; Korfhagen, T. R.; Whitsett, J. A. Activity of pulmonary surfactant protein-D (SP-D) in vivo is dependent on oligomeric structure. *J. Biol. Chem.* **2001**, *276* (22), 19214−19219.
(56) Crouch, E.; Persson, A.; Chang, D.; Heuser, J. Molecular structure of pulmonary surfactant protein D (SP-D). *J. Biol. Chem.* **1994**, *269* (25), 17311−17319.
(57) Wang, F.; Wang, J. N.; He, X. Y.; Suo, X. G.; Li, C.; Ni, W. J.; Cai, Y. T.; He, Y.; Fang, X. Y.; Dong, Y. H.; et al. Stratifin promotes renal dysfunction in ischemic and nephrotoxic AKI mouse models via enhancing RIPK3-mediated necroptosis. *Acta Pharmacol. Sin* **2022**, *43* (2), 330−341.
(58) Hashiba, T.; Suzuki, M.; Nagashima, Y.; Suzuki, S.; Inoue, S.; Tsuburai, T.; Matsuse, T.; Ishigatubo, Y. Adenovirus-mediated transfer of heme oxygenase-1 cDNA attenuates severe lung injury induced by the influenza virus in mice. *Gene Ther.* **2001**, *8* (19), 1499−1507.
(59) Blázquez-Prieto, J.; Huidobro, C.; Lopez-Alonso, I.; Amado-Rodriguez, L.; Martin-Vicente, P.; Lopez-Martinez, C.; Crespo, I.; Pantoja, C.; Fernandez-Marcos, P. J.; Serrano, M.; et al. Activation of p21 limits acute lung injury and induces early senescence after acid aspiration and mechanical ventilation. *Transl. Res.* **2021**, *233*, 104−116.
(60) Jahani, M.; Dokaneheifard, S.; Mansouri, K. Hypoxia: A key feature of COVID-19 launching activation of HIF-1 and cytokine storm. *J. Inflamm.* **2020**, *17*, 33.
(61) Rizou, M.; Frangou, E. A.; Marineli, F.; Prakoura, N.; Zoidakis, J.; Gakiopoulou, H.; Liapis, G.; Kavvadas, P.; Chatziantoniou, C.; Makridakis, M.; et al. The family of 14−3-3 proteins and specifically 14−3-3sigma are up-regulated during the development of renal pathologies. *J. Cell Mol. Med.* **2018**, *22* (9), 4139−4149.

https://doi.org/10.1021/acs.jproteome.4c00980
J. Proteome Res. 2025, 24, 1941−1955